Coupling Interactions between Voltage Sensors of the Sodium Channel as Revealed by Site-specific Measurements

Baron Chanda,[2] Osei Kwame Asamoah,[1] and Francisco Bezanilla[1,2]

[1]Departments of Physiology and Anesthesiology, David Geffen School of Medicine at University of California, Los Angeles, CA 90025
[2]Centro de Estudios Cientificos, Valdivia, Chile

ABSTRACT The voltage-sensing S4 segments in the sodium channel undergo conformational rearrangements in response to changes in the electric field. However, it remains unclear whether these structures move independently or in a coordinated manner. Previously, site-directed fluorescence measurements were shown to track S4 transitions in each of the four domains (Chanda, B., and F. Bezanilla. 2002. *J. Gen. Physiol.* 120:629–645). Here, using a similar technique, we provide direct evidence of coupling interactions between voltage sensors in the sodium channel. Pairwise interactions between S4s were evaluated by comparing site-specific conformational changes in the presence and absence of a gating perturbation in a distal domain. Reciprocity of effect, a fundamental property of thermodynamically coupled systems, was measured by generating converse mutants. The magnitude of a local gating perturbation induced by a remote S4 mutation depends on the coupling strength and the relative equilibrium positions of the two voltage sensors. In general, our data indicates that the movement of all four voltage sensors in the sodium channel are coupled to a varying extent. Moreover, a gating perturbation in S4-DI has the largest effect on the activation of S4-DIV and vice versa, demonstrating an energetic linkage between S4-DI and S4-DIV. This result suggests a physical mechanism by which the activation and inactivation process may be coupled in voltage-gated sodium channels. In addition, we propose that cooperative interactions between voltage sensors may be the mechanistic basis for the fast activation kinetics of the sodium channel.

KEY WORDS: cooperativity • sodium channel • gating • fluorescence • conformational changes

INTRODUCTION

The voltage-dependent sodium channel, which is responsible for the rising phase of an action potential, is a single polypeptide with four homologous domains. In contrast, voltage-dependent potassium channels are comprised of four subunits, each one similar to an individual domain of the sodium channel. The divergence in the primary structure between sodium-channel domains is expected to confer functional distinctions. Indeed a number of structure-function studies have revealed that the voltage sensors of Na^+ channels have discrete functions (Stuhmer et al., 1989; Chen et al., 1996; Kontis and Goldin, 1997; Kontis et al., 1997; Chanda and Bezanilla, 2002). In the present study, we address the issue of cooperative interactions between the four voltage sensors of the sodium channel.

Each domain of the sodium channel contains a highly conserved fourth transmembrane segment, otherwise known as the S4, in which every third residue is positively charged (Stuhmer et al., 1989; Yang and Horn, 1995; Yang et al., 1996). This structure is recognized as the primary voltage sensor in the superfamily of voltage-gated ion channels (Liman et al., 1991; Papazian et al., 1991; Aggarwal and MacKinnon, 1996; Noceti et al., 1996; Seoh et al., 1996). In their landmark paper, Hodgkin and Huxley (1952) demonstrated that the macroscopic current behavior of the sodium channel can be adequately described by a model in which three gating particles control the opening of the channel, and a fourth particle modulates the inactivation process. The gating particles and inactivation unit were postulated to move independently upon membrane depolarization. However, subsequent studies revealed that inactivation is dependent on the state of activation (Goldman and Schauf, 1972; Armstrong and Bezanilla, 1977; Aldrich et al., 1983; Aldrich and Stevens, 1983). Successive models incorporated coupled behavior of the inactivation lid (West et al., 1992; Patton et al., 1993), which closes the ion conduction pathway, with independent movement of the voltage sensors (Armstrong and Bezanilla, 1977; Keynes and Kimura, 1983; Patlak, 1991). On the other hand, more recent kinetic models of the sodium channel based on gating, ionic, and single-channel recordings have proposed modest interactions between gating particles to account for identical rate constants in early transitions (Vandenberg and Bezanilla, 1991). Alternative models of so-

Baron Chanda and Osei Kwame Asamoah contributed equally to this work.

Address correspondence to Dr. Francisco Bezanilla, Departments of Physiology and Anesthesiology, David Geffen School of Medicine at UCLA, 650 Charles E. Young Dr. South, Los Angeles, CA 90025. Fax: (310) 794-9612; email: fbezanil@ucla.edu

dium channel gating have also invoked cooperative interactions between initial transitions of the S4s to account for the slow-rising phase of gating currents (Keynes and Elinder, 1998).

A number of detailed studies on cooperativity between channel subunits have been performed on K_v and K_{Ca} channels (Smith-Maxwell et al., 1998; Horrigan and Aldrich, 1999; Horrigan et al., 1999; Ledwell and Aldrich, 1999). The homotetrameric nature of potassium channels reduces the number of interactions and states, therein, greatly simplifying the analysis. In contrast, deciphering coupling mechanisms in a multidomain and a functionally asymmetric protein like the sodium channel is challenging due to the global nature of the measured parameter. The global parameter, such as ligand binding or channel opening, encapsulates the individual contributions from each domain, and, thus, cannot uniquely define the contributions of each subunit. A more substantial limitation of this approach is that the measured global quantity may not reveal the true pattern of cooperative interactions operating at the site-specific level. For instance, it can been shown that even for a simple model consisting of two interacting nonidentical binding sites, a positive interaction between the sites may be manifested as apparent negative cooperativity in a global description (Di Cera, 1998). Thus, site-specific analysis is of fundamental importance in dissecting the molecular nature of cooperative interactions.

The aim of the present study is to investigate whether cooperativity is manifested at the level of voltage-sensor movement in the sodium channel. For this purpose, we monitored the kinetics and voltage dependence of the fluorescently tagged S4 in the presence and absence of distal gating perturbations. Converse double mutants were also examined to test the reciprocity of effects. Our results indicate that perturbation-induced shifts in S4 movement are a function of interdomain coupling energetics and equilibrium positions of paired voltage sensors along the voltage axis. These experiments provide direct experimental evidence for cooperativity between the voltage sensors of the sodium channel.

MATERIALS AND METHODS

Modified Cut Open Oocyte Epifluorescence Setup

The modified cut open setup used to measure the voltage-dependent fluorescence signals has been described previously (Cha and Bezanilla, 1998). The cut open oocyte configuration allows for spatial voltage homogeneity and fast temporal resolution. The setup is placed on the stage of an upright microscope (BX50WI; Olympus Optical) and the light was focused using a LumPlanFl 40X water-immersion objective (0.8 NA). The light from a tungsten halogen light source was filtered with 535DF35 and split using a 570DRLP dichroic mirror. The excitation light was triggered with a VS25 shutter (Vincent Associates). The emitted light passed through a 565EFLP longpass filter (Chroma Technologies and Omega Optical). This emitted light was then focused onto a PIN-020A photodiode (UDT Technologies) by a microscope condenser lens. The photodiode was connected to the headstage of an integrating Axopatch 1B patch clamp amplifier (Axon Instruments, Inc.). The current from the photodiode was offset to prevent saturation of the feedback capacitor during acquisition.

Data Acquisition

Electrical and optical signals were acquired in two independent channels and digitized on two 16 bit A/D converters in a PC44 board (Innovative Integration). When the data was sampled at intervals longer than 5 μs, the program acquired the data at 5 μs/point, digitally filtered them to the new Nyquist frequency, and decimated them to the new sampling frequency; fluorescence and current were acquired at cut-off frequencies of 20 and 10 kHz, respectively. The data acquisition and analysis programs were developed in-house. For ionic current measurements, linear leak and membrane capacitive current were subtracted using a standard online P/4 procedure. Each fluorescence recording is an average of 20 traces generated by a depolarizing pulse of 20 ms to a test potential after a −130-mV prepulse of 200 ms from a holding potential of −80 mV. The external and internal solutions contained 115 mM N-methylglucamine-methylsulfonate (NMG-MES) to minimize series resistance errors. As a result, the measured ionic currents are only outward due to the flux of residual internal potassium through the sodium channel.

Molecular Biology, Expression, and Labeling

The α subunit of the rSKM1 was cloned into a PBSTA vector optimized for oocyte expression as described previously (Chanda and Bezanilla, 2002). This DNA, which was used as a template for all subsequent mutagenesis, contains three additional silent mutations that generate unique restriction sites. Site-directed mutagenesis was performed using a two-step PCR protocol. The PCR fragments containing the mutation were cloned into unique restriction sites and sequenced to confirm the mutation. The α subunit of the Na channel and the β-subunit cRNA were transcribed from Not-I linearized cDNA in vitro with T7 polymerase (Ambion, Inc.). A 50-ng sample of cRNA, with the α and β mixed in 1:2 molar ratio, was injected. The oocytes were incubated for 4–7 d after injection at 18°C in a incubation solution of 100 mM NaCl, 2 mM KCl, 1.8 mM $CaCl_2$, 1 mM $MgCl_2$, 5 mM HEPES, 10 μM EDTA, and 100 μM DTT. The oocytes were labeled on ice in a depolarizing solution with 5 mM of 5′-tetramethylrhodamine (Cat # T6027; Molecular Probes) for 30–45 min.

Data Analysis

Plots of the voltage dependence of S4 fluorescence (or F-V) were generated by measuring the amplitude of the optical signal (typically after 20 averages) with depolarizing pulses to a range of potentials. F-V curves were normalized to the maximal value to facilitate gating comparisons between mutant channels. Although the TMRM signal near the S4 of each domain is characterized by two kinetic components (Chanda and Bezanilla, 2002), the fast component that correlates to S4 movement makes the major contribution to the amplitude. Thus, the fluorescence-voltage curves were fit to a first order Boltzmann function of the form

$$\frac{F}{F_{\max}} = \frac{1}{1 + \exp[-ze(V - V_{1/2})/kT]}.$$

$V_{1/2}$ is the midpoint of activation of the subunit, z is the valence, kT has its usual thermodynamic meaning, e is the electronic charge, and ze/kT is the slope factor.

A customized Windows-compatible data analysis program was used to construct the F-V curves from the optical signals. Gating

parameters were obtained from Boltzmann fits of the fluorescence using SigmaPlot 8 (SPSS, Inc.) and Excel 2000 (Microsoft). Simulations of the induced gating shifts in the cooperative four state model were generated by Berkeley Maddona (University of California, Berkeley, CA).

RESULTS

Experimental Strategy

Cysteine residues introduced near the S3-S4 extracellular linker of the sodium channel labeled with tetramethylrhodamine have been shown previously to track voltage-sensor movement (Chanda and Bezanilla, 2002). In particular, the fluorescence signals from these sites near domains I, II, and III are highly correlated with the fast component of gating charge, and, thus, are sensitive reporters of S4 conformational changes. Fig. 1 A shows an alignment of the fourth transmembrane segments from each domain of the rat skeletal muscle sodium channel where the engineered cysteines are designated by stars. The gating perturbations used in this work were motivated by previous studies that demonstrated robust conductance-voltage (g-V) shifts in charge-reversal and charge-neutralization mutations of S4 gating residues (Stuhmer et al., 1989; Chen et al., 1996; Kontis et al., 1997) (Table I). We tested the functional effect of many charge mutations (Fig. 1 A, circles) with site-specific fluorescence measurements. Thus, the sodium channels employed in this study contain two classes of mutations: (a) mutated cationic S4 residues that induce gating perturbations; and (b) fluorophore-conjugated cysteine residues that track S4 movement.

Our experimental strategy is as outlined in Fig. 1 B. The local effect of the gating perturbation was initially characterized by comparing the optical signature of a TMRM-labeled residue in the presence (second schematic, top of Fig. 1 B) and absence (first schematic, top of Fig. 1 B) of a gating charge mutation within the same domain. Those gating mutations that produced substantial effects were subsequently engineered into channels containing a fluorophore placed in a distal S4 segment (bottom of Fig. 1 B, second schematic). As the eukaryotic sodium channel is comprised of four voltage sensors, a minimum of six pairwise mutants (each containing one perturbed domain and one TMRM-labeled domain) is required to completely determine all possible combinations. Since conservation of free energy mandates reciprocity between coupled processes, converse pairwise mutants, in which the location of the perturbed and fluorescent domains are interchanged, were also tested (Wyman and Gill, 1990).

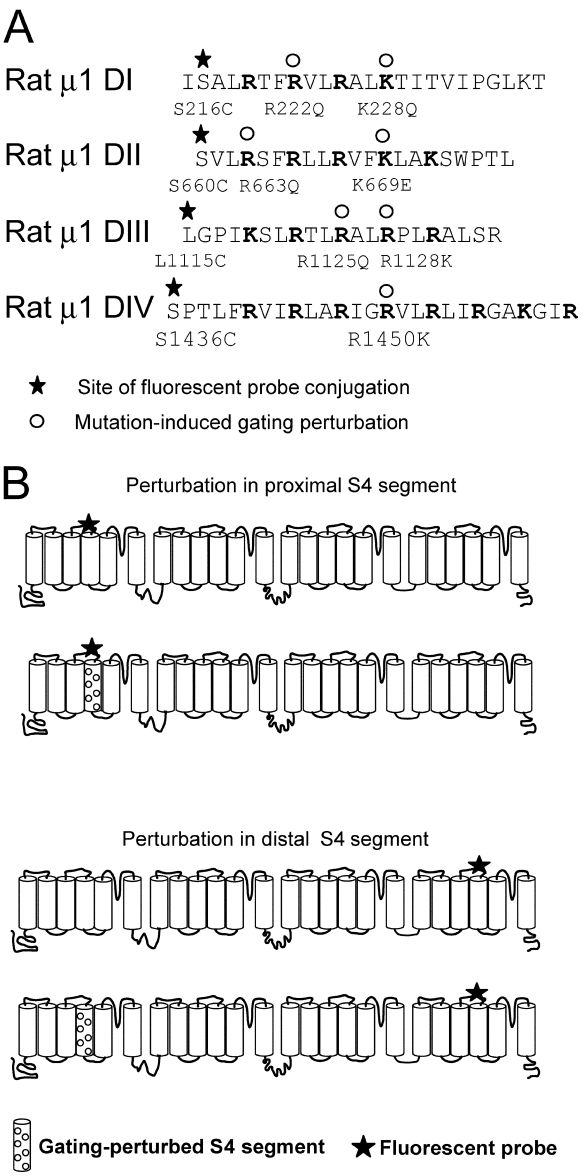

FIGURE 1. Primary structure of S4 segments and experimental design. (A) Sequences of the four S4 segments are shown to illustrate the cysteine-modification sites (stars) and all gating charge mutations (open circles) including those that did not yield fluorescence voltage shifts (see experimental strategy section in RESULTS). (B) The gating perturbation is initially characterized by introducing a mutation in the same S4 in which the fluorescent probe is located (top). The gating perturbations demonstrating the largest local effects are then introduced into "chimeric" channels containing a fluorescent probe in a different domain (bottom). The monitoring site is labeled as a star and the perturbed segment is shown with open circles.

Characterization of Gating Perturbations

For the remainder of the paper, double mutants containing a gating perturbation and fluorophore within the same S4 will be denoted by using either the standard notation or an abbreviated label. In the latter case, the charge perturbation is designated by a degree symbol while an asterisk denotes the TMRM-labeled residue. Thus, R228Q-S216C mutant, where the charge

TABLE I

Conductance and Fluorescence Properties of Gating Perturbing Mutations

	Conductance		Fluorescence	
	Midpoints of activation	Slope	Midpoints of activation	Apparent slope
	mV		*mV*	
Wild-type[¶]	−31.9[¶], −32.7[‡]	5.6[¶], 6.3[‡,Ω]		
S216C			−67.1	1.3
S660C			−58.3	1.0
L1115C			−75.9	1.2
S1436C			−70.8	1.1
R222Q[§,‡]	−30.1[§], −40[‡]	5.5[§], 4.5[‡,Ω]		
R222Q-S216C			−68.8	0.9
K228Q[§,‡]	−10.6[§], −13[‡]	3.9[§], 5.4[‡,Ω]		
K228Q-S216C			−15.0	1.02
R663Q[¶]	−18.6[¶]	4.4[¶]		
R663Q-S660C			28.1	1.2
R672Q[§]	−14.2[§]	4.4[§]		
R672Q-S660C			−44.3	0.9
R1125Q[¶]	−26[¶]	3.5[¶]		
R1125Q-L1115C			−56.6	1.09
R1128Q[§]	−47.2[§]	5.4[§]		
R1128Q-L1115C			−68.6	1.3
R1128K[§]	−19.3[§]	4.5[§]		
R1128-L1115C			−79.4	1.1
R1450K[§]	−21.7[§]	5.7[§]		
R1450K-S1436C			−38.7	1.3

Fluorescence parameters of mutants obtained from fits of the F-V to a first order Boltzmann function. The data from each mutant represents a fit to the mean of 3–5 oocytes.

[¶]Kontis et al., 1998.

[§]Chen et al., 1996.

[‡]Stuhmer et al., 1989.

[Ω]The values of slope from Stuhmer et al. (1989) were multiplied by three since those values were for a single gating charge assuming three identical gating charges.

and cysteine mutation are both located in domain I will be depicted as DI°-DI*.

For comparison, the time course of fluorescence change during a depolarizing pulse in the presence (gray) and absence (black) of gating charge mutations are shown in Fig. 2 A. Fluorescence traces were normalized with respect to the maximal value recorded at depolarized potentials. The most dramatic effect is see on DII°- DII* mutant (second column, gray trace), which exhibits a small fluorescence change at −10 mV, whereas the signal representing the unperturbed mutant, DII* (second column, black trace), is almost maximal in amplitude. The effect of gating perturbation is clearly apparent in the time course of fluorescence change in all the domains, especially at small depolarizations.

The magnitude of gating perturbations is quantitated by plotting the steady-state fluorescence signal with respect to membrane potentials in the presence (gray) and absence (black) of gating charge perturbations (Fig. 2 B). The parameters of fluorescence voltage curves for perturbed and unperturbed cysteine mutants are summarized in Table I and were obtained by fitting the data to a single Boltzmann distribution. Among all of the intradomain gating mutants, mutation of R663 to glutamine in the S4 of second domain exerts the largest perturbation on voltage sensor movement (from $V_{1/2} = -58.3$ to +28.1 mV, Fig. 2 B). Mutation of the third residue in domain I (DI°-DI*) shifts the fluorescence-voltage curve from $V_{1/2} = -67.1$ mV to a new mean value ($V_{1/2} = -15.0$ mV, $z = 1.02e_o$). The largest shift (+20 mV) for a perturbation in domain III is seen on mutation of the third charge whose F-V relation is shown Fig. 2 B (third graph). In the fourth domain, a charge conservative (R1450K) mutation produces a 31-mV shift in the fluorescence voltage curve. This substantial gating perturbation suggests that this residue likely serves a structural role in stabilizing the activated state with respect to the deactivated state. The physical basis for the large perturbations in voltage sensor gating on other domains cannot be unambiguously determined. If the effect of arginine neu-

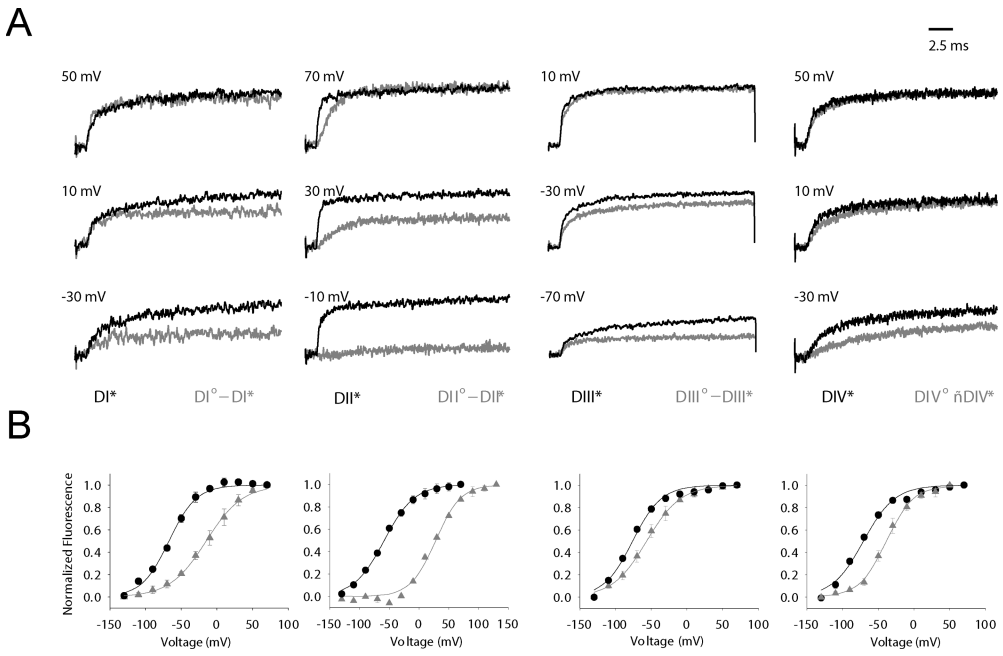

FIGURE 2. Gating charge perturbations modify voltage sensor movement. (A) The black fluorescence traces represent TMRM-labeled cysteine residue in the "wild-type" S4 domain while the gray represent signals from the double mutant comprised of the gating charge perturbation and TMRM-conjugated cysteine within the same voltage sensor. The following voltage clamp protocol was used: holding potential = −80 mV, oocytes were pulsed from −130 mV (D1 = 400 ms) to the indicated potential for 20 ms, then returned to −130 mV for a total cycle period of 2 s. For each domain pair, the optical signals are normalized to the maximum value to facilitate amplitude comparison. (B) The voltage-dependent fluorescence signal of the "perturbed" domains are shifted toward depolarized potentials relative to "wild-type" domains. The mean of the normalized fluorescence change (at 20 ms) for the unperturbed domains (black) and gating-charge perturbed domains (gray) were fit to a single Boltzmann function.

tralizations is simply a reduction in the number of charge-carrying residues, then the slope of the F-V curve may be diminished without an effect on the midpoint of activation. However, most of the perturbations used in this study dramatically shift the midpoint of activation of each S4 segment with minimal effect on the slope factor; therefore, the perturbation influences the voltage-independent (or chemical) component of the equilibrium constant. In other words, the perturbation effects are likely a result of disrupted structural interactions that destabilize the activated conformational state shifting the F-V curves toward depolarized potentials.

Gating charge perturbation in each domain does not modulate the S4 movement (F-V) and conductance (g-V) to an equivalent extent (Table I). For instance, in the second domain, R663Q mutation displaces the g-V curve to the right by 11 mV, which is comparable to the 15-mV shift produced by the R672Q mutation. The optical data, in contrast, shows that the F-V curve is right shifted by 85 mV in the R663Q mutation as compared with only 14 mV in R672Q. In the case of the third domain, the charge conservation mutation R1128K shifts the conductance-voltage (g-V) curve in the hyperpolarizing direction by 12 mV, whereas the F-V curve is essentially unchanged. The remaining mutations used in this study shifted both fluorescence and conductance parameters yet the optical signals were consistently displaced to a much greater degree. This difference in the magnitude of the g-V and F-V perturbations may reflect that conductance is a product of the activated probability of each domain (i.e., F-V), such that relatively large shifts in S4 gating produce only modest shifts in conductance parameters (Hodgkin and Huxley, 1952). Alternatively, the discrepancy between the optical and electrophysiological parameters may indicate that individual domains contribute differentially to the conducting state of the channel (Hanck and Sheets, 1995). While identifying the precise gating steps affected by the charge mutations is beyond the scope of this work, a combination of single channel and gating current data with site-specific measurements may help us elucidate the role of particular S4 charges and the effect of their mutations.

Gating Perturbations in One Domain Affect the Operation of other Domains

Site-specific fluorescence measurements have been used to dissect cooperative interactions in voltage-gated ion channels (Mannuzzu and Isacoff, 2000). However, unlike this prior study on the multimeric Shaker K channel, where the precise stoichiometry of the perturbed and labeled subunits were difficult to ascertain, the voltage-gated sodium channel affords one primary advantage. The covalently linked domains of the sodium channel ensure a uniform population of channels, each containing only one gating-perturbed domain and a single TMRM fluorescent reporter. Thus, to determine whether S4 movement is cooperative, we

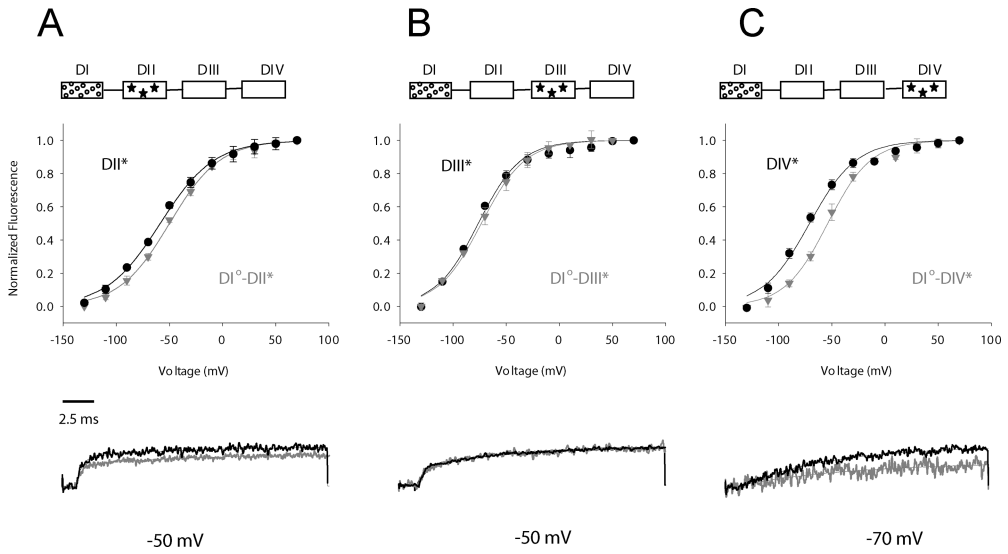

FIGURE 3. Interdomain interactions of a perturbed first domain as revealed by shifts in the voltage dependence of S4 movement. (Inset) Generic diagram of sodium channel depicting the domain in which the gating-charge perturbation (open circles) and the fluorescent-tagged domain (stars) are located. (Top) In all cases, wild-type domain movement is shown in black circles relative to domain movement in the presence of a distal gating perturbation (gray inverted triangles). A gating charge perturbation in domain I (K228Q) destabilizes the activated conformation of the S4 in domains II (S660C, panel A) and IV (S1436C, panel C), but has no apparent effect on domain III (L1115C, panel B). (Bottom) A selected sweep of "wild-type" and "chimeric" domains are shown for comparison at the voltage in which the greatest difference in kinetics or amplitude was observed.

generated a set of double mutants or chimeric channels where the gating mutation and TMRM-conjugated cysteine residue are located in different voltage sensors. The gating perturbations that exhibited the largest shifts (refer to Table I) were used in these chimeric channels.

The lower portion of Fig. 3 compares the evoked fluorescence of domain I chimeras containing the K228Q gating mutation with a TMRM probe in domain II (A), III (B), or IV (C) (gray traces) to the respective wild-type S4 movement (black traces). While the kinetics of S4 activation in domains II and III are only nominally affected by the gating perturbation in the first domain, the K228Q neutralization significantly slows the activation time course of S4-DIV (bottom of Fig. 3 C). Accordingly, domain I exerts the maximal effect (30-mV depolarizing shift) on the fourth domain's voltage sensor (DI°-DIV*) (top of Fig. 3 C), whereas a minimal effect or none at all is induced in the second and third domains (Fig. 3, A and B, top), respectively. Generic illustrations of the sodium channel are shown in the insets to clarify the location of the gating perturbation

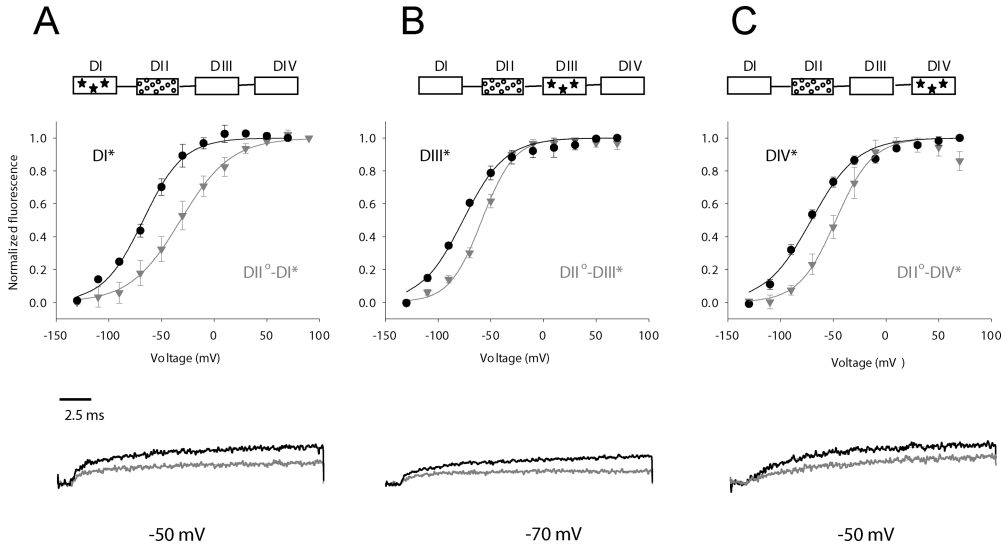

FIGURE 4. Interdomain interactions of a perturbed second domain as revealed by shifts in the voltage dependence of S4 movement. (Top) As in Fig. 3, the "wild-type" domain movement is shown in black circles relative to domain movement in the presence of a distal gating perturbation (gray inverted triangles). Gating charge perturbations in domain II (R663Q) destabilize the activated conformation of the S4 in domains I (S216C, panel A), DIII (L1115C, panel B), and domain IV (S1436C, panel C). (Inset) The box diagrams have the same meaning as in Fig. 3. (Bottom) Once again a selected sweep illustrating the difference between the two mutants is provided.

TABLE II

Fluorescence Characteristics of Distal Domain Gating Perturbations

Mutants	Midpoint of activation ($V_{1/2}$)	Apparent slope (z)
	mV	
K228Q-S660C (DI°-DII*)	−49.5 ± 5.04	1.1 ± 0.12
K228Q-L1115C (DI°-DIII*)	−80.2 ± 1.46	1.93 ± 0.10
K228Q-S1436C (DI°-DIV*)	−53.7 ± 3.41	1.25 ± 0.05
R663Q-S216C (DII°-DI*)	−30.0 ± 7.5	1.1 ± 0.13
R663Q-L1115C (DII°-DIII*)	−58.8 ± 1.9	1.69 ± 0.14
R663Q-S1436C (DII°-DIV*)	−47.4 ± 5.98	1.5 ± 0.04
R1125Q-S216C (DIII°-DI*)	−49.0 ± 4.49	0.95 ± 0.1
R1125Q-S660C (DIII°-DII*)	−46.1 ± 6.85	1.15 ± 0.04
R1125Q-S1436C (DIII°-DIV*)	−61.9 ± 1.71	1.29 ± 0.05
R1450K-S216C (DIV°-DI*)	−27.2 ± 5.16	1.18 ± 0.16
R1450K-S660C (DIV°-DII*)	−42.9 ± 6.8	1.26 ± 0.09
R1450K-L1115C (DIV°-DIII*)	−65.5 ± 6.6	1.31 ± 0.13

Fluorescence parameters of "chimeric" mutants obtained from fits of the F-V to a first order Boltzmann function. The data from each mutant represents a fit to the mean of 3–5 oocytes.

(circles) and fluorophore-tagged domain (stars). The differential effect of the domain I gating mutation on S4 movement in domain II, III, and IV are consistent with specific interdomain interactions rather than a global effect of the mutation.

In Fig. 4, fluorescence voltage curves from double mutants containing the R663Q gating perturbation (in S4-DII) and a fluorophore in either domain I(A), domain III(B) or domain IV(C) are compared. The R663 charge neutralization displaces S4-DI movement by 30 mV toward depolarized potentials (Fig. 4 A). As this chimera is a converse of the DI°-DII* mutant (Fig. 3 A), an equivalent induced shift may be expected at first approximation. However, as we will show later, this apparent discrepancy in the measured perturbation between two reciprocal pair-wise mutants reflects the influence of equilibrium positions of these voltage sensors. This arginine neutralization in the second domain also modulates S4-DIII gating (~17 mV in Fig. 4 B). Finally, the voltage sensors in the second and fourth domain are coupled as evidenced by a shift of 22 mV (Fig. 4 C) in F-V of DII°-DIV*. Interestingly, a gating charge perturbation in S4-DII not only modulates the midpoint of activation of distal voltage sensors, but also alters their apparent valence (Table II). This may reflect disrupted electrostatic interactions between the native cationic residues and proximal charged amino acids with a resultant reshaping of the electric field through which the gating charges move.

Next, we explored the effect of the R1125Q gating perturbation in S4-DIII on the movement of other S4s (Fig. 5). The DIII°-DI* mutant with a TMRM reporter in the first domain exhibits an 18-mV shift in $V_{1/2}$ toward positive potentials relative to the intrinsic S4–domain I position (top of Fig. 5 A). Notice that the foot of the F-V curve is not displaced in this instance indicating that the gating perturbation in the third domain is likely to affect the activated state much more than the resting state. This phenomenon is not observed in the interactions between domains II and III or domains III and IV although moderate shifts are observed in both cases (Fig. 5, B and C, top). The bottom of Fig. 5 shows representative fluorescence traces from chimeric channels at a single test potential containing R1125Q gating perturbation.

The S4 of the fourth domain is believed to be uniquely involved in coupling the activation process to the inactivation gate (Hanck and Sheets, 1995; Sheets

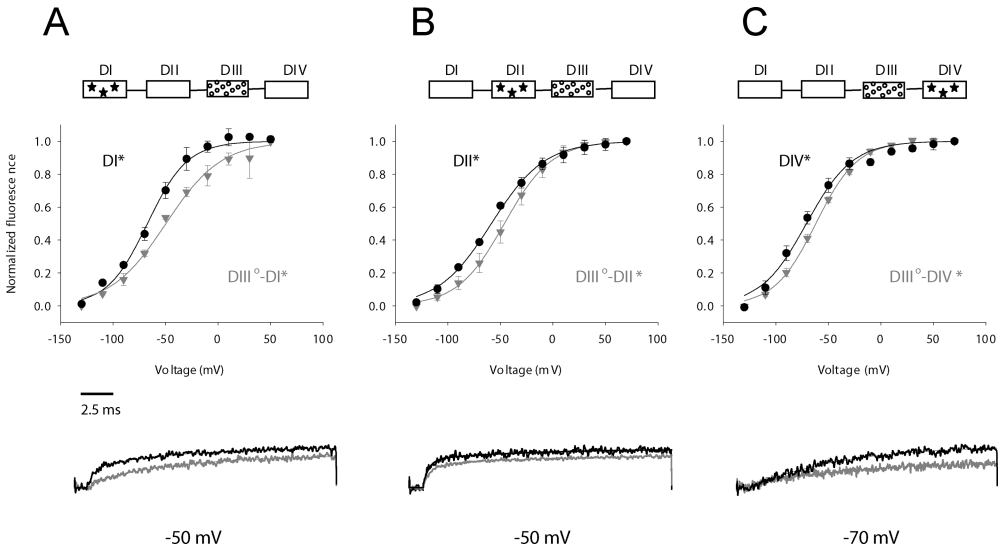

FIGURE 5. Inter-domain interactions of a perturbed third domain as revealed by shifts in the voltage-dependence of S4 movement. The wild-type domain movement is shown in black circles relative to domain movement in the presence of a distal gating perturbation (gray inverted triangles). Gating charge perturbations in domain III (R1125Q) destabilize the activated conformation of the S4 in domains I (S216C, panel A), DII (S660C, panel B), and domain IV (S1436C, panel C). (Inset) The box diagrams have the same meaning as in the previous figures. (Bottom) Selected sweeps for comparison.

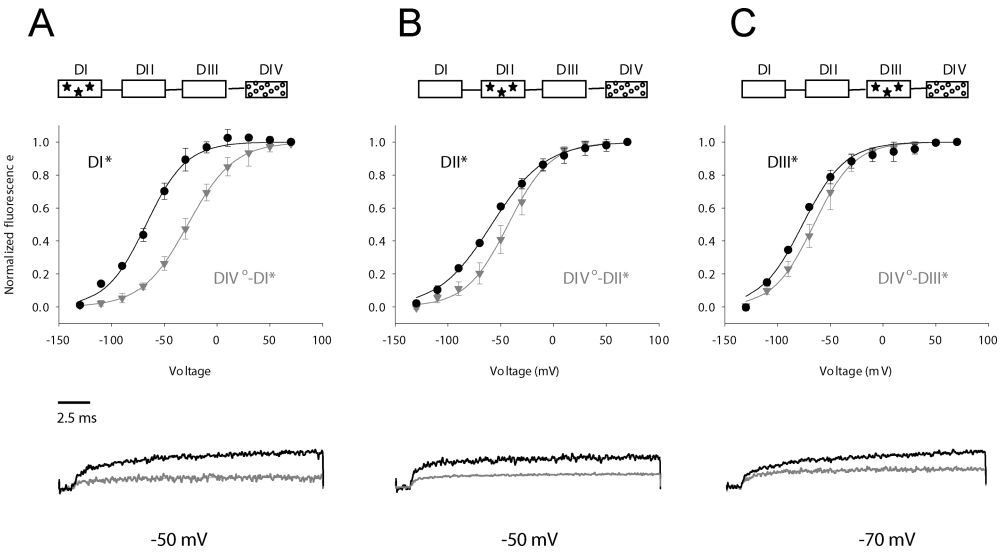

FIGURE 6. Interdomain interactions of a perturbed fourth domain as revealed by shifts in the voltage dependence of S4 movement. As in the previous figures, the wild-type domain movement is shown in black circles relative to domain movement in the presence of a distal gating perturbation (gray inverted triangles). Gating charge perturbations in domain IV (R1125Q) modulate the S4 movement in domains I (S216C, panel A), DII (S660C, panel B), and domain III (L1115C, panel C). (Inset) The generic diagram is as described in Fig. 3.

and Hanck, 1995; Chen et al., 1996; Mitrovic et al., 1998; Cha et al., 1999; Sheets et al., 1999; Catterall, 2000; Mitrovic et al., 2000; Chanda and Bezanilla, 2002). We have shown previously that the activation of S4-DIV occurs relatively late in the activation sequence and may be facilitated by fast S4 transitions in domains I, II, or III (Chanda and Bezanilla, 2002). A gating perturbation in the fourth domain induces a large displacement in the F-V of S4-DI (DIV°-DI*) ($\Delta V_{1/2}$ = +39 mV) and relatively modest shifts in S4-DII (DIV°-DII*) ($\Delta V_{1/2}$ = +15 mV) and S4-DIII (DIV°-DIII*) ($\Delta V_{1/2}$ = 10 mV). A comparison of the activation time course of these different voltage sensors in the presence and absence of the S4-DIV gating perturbation is shown at the bottom of Fig. 6. These results indicate that the voltage sensor of domain IV is coupled to the S4 segments of other domains, most notably the S4 of domain I.

Effect of Distal Perturbation Depends on Coupling Strength and Relative Equilibrium Positions

The cumulative results from the perturbation experiments are presented in terms of shifts in midpoint of activation ($\Delta V_{1/2}$) for the chimeric mutants as summarized in Fig. 7 (and Table II). The data reveals two important attributes of inter-domain cooperativity in the sodium channel. First, gating perturbations in one do-

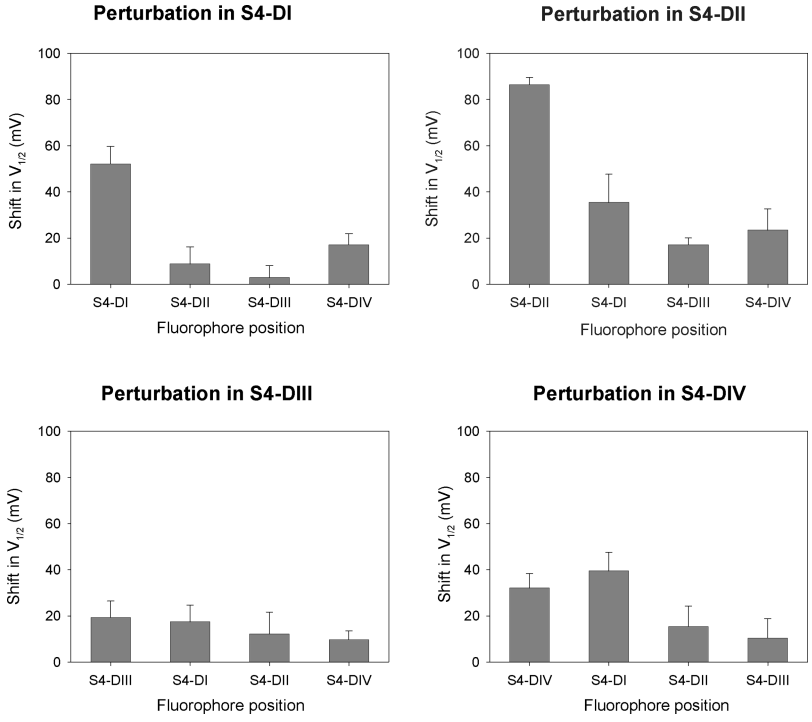

FIGURE 7. Shifts in the activation midpoints due to a gating perturbation. The activation shift is the difference between activation midpoints ($V_{1/2}$) of the perturbed domain versus the unperturbed domain. The error bars represent standard error and were calculated using the equation $s^2 = s_A^2 + s_B^2$. The s_A and s_B are the standard deviations of two variables A and B that in this case represent the activation midpoints of the perturbed and the unperturbed domain. Each panel summarizes data from a common set of double mutants where the perturbation is localized in one particular domain. The fluorophore position in each of these double mutants is indicated on the y-axis.

main can greatly modulate the voltage-dependent behavior of distal S4 segments. For instance, a gating mutation in S4-DIV (R1450K) that induces a shift in S4-DI movement ($\Delta V_{1/2} = +39$ mV) is approximately equal in magnitude (within error) to the measured shift of its own domain ($\Delta V_{1/2} = +32$ as measured by DIV°-DIV*). Similarly, a charge perturbation in the second domain (R663Q) exerts a 37-mV midpoint shift in domain I movement (DII°-DI*); this long-range effect is ~50% of the intradomain perturbation as reflected by the midpoint of activation of "wild-type" S4-DII versus DII°-DII*. Second, the magnitude of $V_{1/2}$ shifts in a converse double mutant pair are not equivalent. This finding was not initially anticipated because thermodynamic considerations dictate that the energetic effects between an interacting pair should be reciprocal. Therefore, we explored this issue by implementing a simple cooperative model of an ion channel that is readily generalizable to models of greater complexity.

The four-state model shown in Scheme I represents a two subunit protein in which each subunit undergoes a single gating transition.

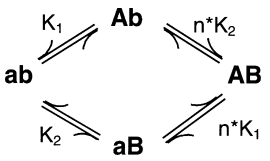

SCHEME I

The **ab** state represents the fully deactivated channel where both subunits are at rest and **AB** represents both subunits in an activated state. Each subunit undergoes a single transition described by a forward ($k_f(V)$) and backward ($k_b(V)$) rate constant according to the expressions:

$$k_f(V) = \exp[q(V - V_{1/2})/kT]$$

$$k_b(V) = \exp[-q(V - V_{1/2})/kT],$$

where q is the subunit charge which was set to $2e_o$, V is the membrane voltage, $V_{1/2}$ is the mid-point of activation for the subunit, and kT has its usual thermodynamic meaning. The equilibrium constants are $K_1 = k_fA(V)/k_bA(V)$ for subunit A and $K_2 = k_fB(V)/k_bB(V)$ for subunit B. Positive cooperativity was integrated into this model by multiplying the forward rate constant of one subunit with a coupling term (n) when the other subunit of the channel was in the activated position. The coupling term was set to a value of 10^6, which is equivalent to a free energy of 8.5 Kcal/mole. The fluorescence-voltage relationship for each subunit was determined numerically by calculating the steady-state population of each state at various potentials and then plotting all states with an activated subunit A or activated subunit B as a function of voltage to represent the F-V of A and B, respectively. Finally, to determine the reciprocity of the perturbation effect, A was initially assigned a $V_{1/2} = -45$ mV, whereas the $V_{1/2}$ of subunit B was set to +30 mV, such that domain A was positioned to the "left" with respect to domain B. Subunit A was then "perturbed" toward depolarized potentials to a $V_{1/2} = +13$ mV, whereas the subunit B's assigned value remained constant. The converse mutant pair was then modeled by shifting the $V_{1/2}$ of subunit B to +67 mV while keeping the assigned value of subunit A constant.

The steady-state properties of the four-state ion channel along with the differential effect of perturbations is shown in Fig. 8. Note that the assigned midpoint potentials of activation are not equivalent to the observed values due to coupling energetics. Subunit A was assigned a $V_{1/2}$ value of −45 mV and its observed value was −52 mV, whereas subunit B was assigned a value of +30 mV and observed $V_{1/2}$ was −50 mV. The simulated data shows that the F-V relationship of A is perturbed to a much smaller extent when the mutation is introduced in B, in contrast to the converse situation (compare induced shifts in Fig. 8, A vs. B). Thus, the magnitude of long-range perturbations is influenced by the relative position of the perturbed versus TMRM-tagged domains.

The effects of distal perturbations in a coupled system can also be understood by examining the steady-state solution relating the measured fluorescence with individual equilibrium constants for the same model (Scheme I). The equilibrium constant of fluorescence activation of a subunit, *i*, is

$$K_i^f = \exp[z_i e_i (V - V_{mi})/kT], \quad (1)$$

where z_i and V_{mi}, the apparent slope and the midpoint of activation, are obtained from the fluorescence data. In this scenario, the equilibrium constant of the fluorescence of one subunit, is given by

$$K_1^f = \frac{(1 + nK_2)K_1}{(1 + K_2)}. \quad (2)$$

A mutation that perturbs K_2 by a factor p will be manifested in the measured fluorescence of subunit 1 as

$$K_{1P}^f = \frac{(1 + npK_2)K_1}{(1 + pK_2)} \quad (3)$$

and from subunit 2 as

$$K_{2P}^f = \frac{(1 + nK_1)pK_2}{(1 + K_1)}. \quad (4)$$

The effect of perturbation is described by perturbation ratio, ρ, which is defined as

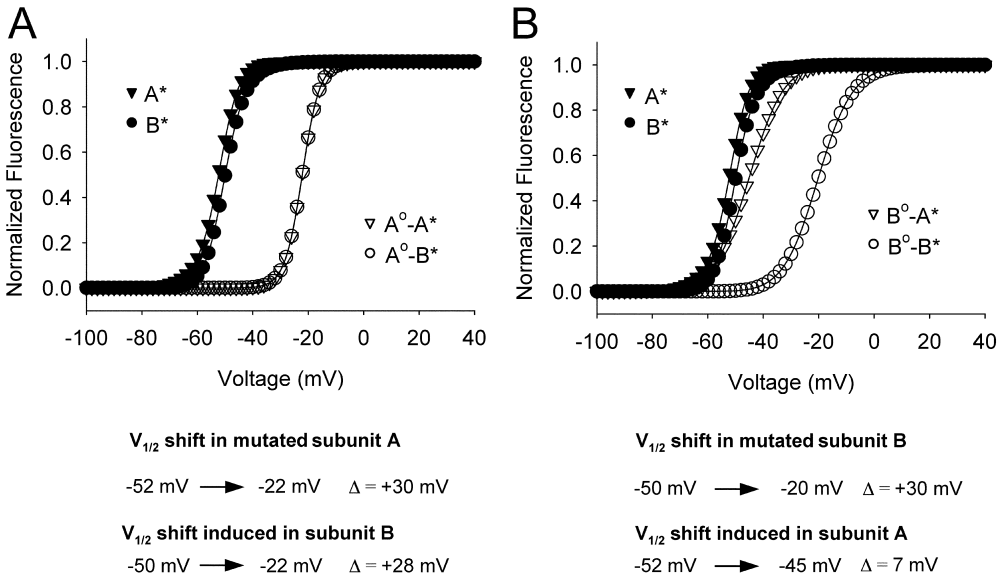

FIGURE 8. Simulated shifts in activation midpoints for a coupled two subunit system depend on their relative positions along the voltage axis. The activation midpoint ($V_{1/2}$) of subunit *A* was initially assigned a value of −45 mV and the $V_{1/2}$ for subunit *B* was +30 mV. As a result of coupling (energy equals to 8.5 kcal/mol), the observed $V_{1/2}$ was −52 mV for *A* and −50 mV for subunit *B*. In panel A, the $V_{1/2}$ of subunit *A* was perturbed to +13 mV, such that the observed $V_{1/2}$ shifts from −52 to −22 mV, a +30-mV shift. The F-V curves of subunits *A* and *B* are superimposed after perturbation, because subunit *B* was shifted by 28 mV. In panel B, the $V_{1/2}$ of subunit *B* was shifted to +67 mV such that the observed $V_{1/2}$ shifts from −50 to −20 mV, again a +30-mV shift. However, the induced shift in subunit *A* was only 7 mV. The induced shifts in the equilibrium values due to the perturbations are also indicated below the figure.

$$\rho = \frac{K_1^f / K_{1P}^f}{K_2^f / K_{2P}^f} = \frac{(1 + pK_2)(1 + nK_2)p}{(1 + npK_2)(1 + K_2)}. \quad (5)$$

When $n = 1$ (no cooperativity), the perturbation ratio,

$$\rho = p. \quad (6)$$

Thus, when $n < 1$(negative cooperativity), $\rho < p$ and when $n > 1$ (positive cooperativity), $\rho > p$.

However, consider the case when $K_2 >> 1$ then

$$K_1^f = nK_1 \text{ and } \rho = p, \quad (7)$$

which is similar to Eq. 6.

Under this condition, a substantial gating perturbation of the second domain (K_2) will not affect the fluorescent properties of the first domain (K_1^f), even when the two domains strongly interact (i.e., large *n* term).

While this two subunit model does not encompass the full complexity of the four-domain sodium channel, the simulation results are consistent with our experimental findings. The fluorescence-voltage curves of S4s in domains III and IV are hyperpolarized shifted with respect to domains I and II. Consequently, large perturbations in the gating properties of first and second domain have a diminished effect on the fluorescence of S4-DIII and S4-DIV (Fig. 7). By extension, relatively small perturbations of the third and fourth domain induce comparatively large shifts in S4-DI and S4-DII. Thus, our experimental findings are consistent with theoretical predictions that the magnitude of long-range inter-domain perturbations are a function of coupling energetics and the relative equilibrium positions of the paired S4 segments.

DISCUSSION

Site-specific fluorescence measurements can reflect either the movement of a tagged S4 segment or the relative rearrangement of proximal quenching groups in a neighboring segment or a composite of both. Gating and ionic current parameters recorded in the same preparation can be used to assign these fluorescence changes to particular physical transitions. Fluorescence data near the S4 segment in Shaker K^+ channel reveals that at most positions optical signal tracks at least one component of gating charge movement (Mannuzzu et al., 1996; Cha and Bezanilla, 1997, 1998; Gandhi et al., 2000; Loots and Isacoff, 2000). Similar studies in the voltage-gated sodium channel reveal that the primary component of the fluorescence signal is conserved between different sites within the same S4 segment. Furthermore, this optical component is well correlated with the time course of gating currents. These results indicate that voltage-dependent fluorescence changes measured near S4 segments reflect voltage-sensor movement. In the present study, we have exploited this attribute in gating perturbed mutants to determine the extent of coupling interactions between different voltage sensors.

Measured Effects Are Due to Long Range Coupling Interactions

Although fluorescence quenching requires close proximity (2 Å or less), it is possible that functional groups

in neighboring domains or subunits may contribute to the optical signal. For example, our fluorescence measurements may report the movement of the tagged S4 relative to a quenching group in the neighboring domain. If this quencher also experiences voltage-dependent changes in position, then a perturbation of this extra-domain quencher may be reflected in the F-V behavior of the labeled S4. This effect, referred to here as a "proximity effect", and its implications are best addressed by examining recent structural models of voltage-gated potassium channels. According to the crystal structure of KvAP channels (Jiang et al., 2003), the S4 segments are outstretched and are unlikely to share contact surfaces with neighboring subunits from the same channel. Thus, in this instance, the fluorescence signal cannot be attributed to a proximity effect. However, an alternative structure of the Shaker channel (Laine et al., 2003) suggests that the S4 lies in close proximity to the S6 segment with a clockwise arrangement of each domain from an extracellular perspective. Supporting evidence for a clockwise arrangement of each domain from an extracellular perspective was provided by molecular footprinting studies of the pore region in the sodium channel using μ-conotoxin (Li et al., 2001). Using Shaker model as a template for the voltage-gated sodium channel, S4-DI is placed adjacent to the S6 of DIV, S4-DII to S6-DI, and so forth. As illustrated in Fig. 9, a TMRM molecule in S4-DI may report structural changes in S6-DIV that are elicited by a S4-DIV gating perturbation. However, this proximity effect will be unidirectional in nature because a fluorophore attached to S4-DIV will be too distant to report local structural changes occurring near S4-DI. In contrast, our results where converse mutation pairs show reciprocal effects are consistent with linked processes (Wyman and Gill, 1990). Furthermore, our measurements reveal that gating perturbations of S4-DIII significantly affect the movement of S4-DI and similar perturbation effects are observed between S4-DII and S4-DIV (Fig. 7). Such distal perturbations observed between voltage sensors assembled on opposite sides of the channel are difficult to explain by only invoking proximity effects. Therefore, we conclude that the effect of distal gating perturbations on voltage sensors of the sodium channel are due to long range coupling interactions.

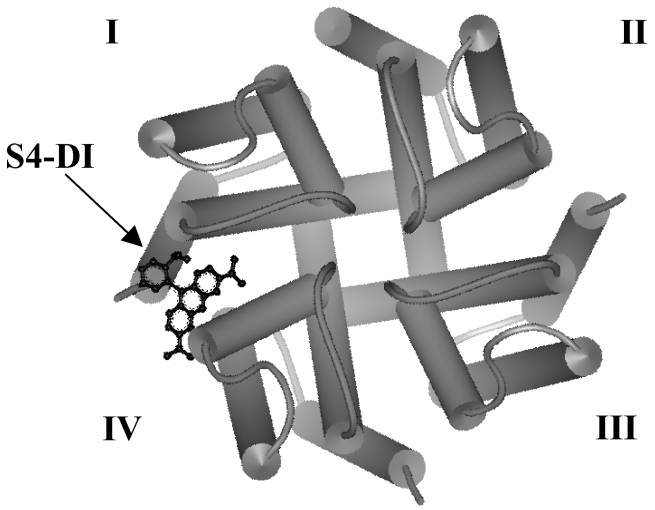

FIGURE 9. Reciprocal perturbation effects in the sodium channel support interdomain cooperative interactions. An extracellular perspective of the KcsA potassium channel is depicted as a structural homologue of the sodium channel. The S4 transmembrane segments were placed at the interface of each domain based on the structure proposed by Laine et al. (2003). In this model, TMRM anchored to S4-DI is placed (arbitrarily) in close proximity to the pore helix of domain IV. Thus, a gating perturbation in S4 of domain IV may modulate the fluorescence signal near S4-DI through a conformational change in the pore helix. However, a perturbation in S4-DI is unlikely to affect a probe attached to S4-DIV in the absence of coupling as the distance between two S4 segments is too large (34 Å). Also, note that the relatively small size of TMRM relative to the dimension of the channel prevents the tethered fluorophore from directly sampling changes in the movement of a neighboring S4.

Divergence of Cooperative Mechanisms in Sodium and Potassium Channels

Among the various kinetic models proposed for the potassium channel, there is a general consensus that activation gating of the potassium channel involves cooperative interactions (Zagotta et al., 1994; Schoppa and Sigworth, 1998). These models envision independently moving voltage sensors during early transitions that converge to a final concerted transition of all subunits for pore opening. In this scenario, how would the perturbation of one voltage sensor affect the movement of the other S4 segments? Horn et al. (2000) showed that immobilization of the voltage sensors of potassium channels with a photocrosslinking reagent did not reveal cooperativity as determined from the relative decrease of gating and ionic currents. However, g-V shifts in tandem heteromultimeric channels suggest cooperativity (Smith-Maxwell et al., 1998). These studies are consistent with the idea that the last step in the activation process is a highly cooperative conformational change that leads to pore opening (Zagotta et al., 1994; Schoppa and Sigworth, 1998). As a result, cooperative interactions in the potassium channel are visible in conductance measurements, but not in gating current measurements. Thus, cooperativity in the K^+ channel is manifested only at the quaternary level between the interacting faces of the subunits (Ledwell and Aldrich, 1999). Similarly, fluorescence studies reveal that the early steps in the activation process are uncoupled as the foot of the F-V curve is unaffected in the presence of a distal gating perturbation (Mannuzzu and Isacoff, 2000). Our measurements in the sodium channel, in

contrast, show that coupling interactions exist during early S4 transitions (for example, shift in foot of F-V of DI°-DIV* and DIV°-DI*). Thus, cooperative interactions are more extensive in the sodium channel such that the voltage sensors likely move in a coordinated manner upon membrane depolarization.

Despite the evidence for cooperativity, the underlying structural basis is only speculative at the present time. In the structural model of the Shaker potassium channel (Laine et al., 2003), coupling may be propagated by an interaction between residues near the S4 with residues in the turret of the neighboring pore. On the other hand, if the crystal structure of the KvAP channel (Jiang et al., 2003) corresponds to the structure in the membrane, the individual S4s have essentially no contact with pore helices of neighboring subunits. In this case interdomain communication is likely to be mediated through contacts between the pore loops, which is the common interaction region. If the structural models of potassium channels are prototypical of all voltage-gated ion channels, how are movements of S4s in the sodium channel coupled unlike potassium channels? We suggest that the major difference between Na^+ and K^+ channels is that the kinetic transitions in the sodium channel are much more tightly coupled as compared with the potassium channel. Thus, in the K^+ channel even when the last transitions are highly coupled the effect is not detected by early transitions, in contrast to the voltage-gated sodium channel studied here. Ultimately, high-resolution structures of voltage-gated K^+ and Na^+ channels will be of immense value in designing experiments to explore the mechanistic basis of S4 coupling.

Functional Role of Cooperativity in the Sodium Channels

Cooperative interactions between S4 segments of the eukaryotic sodium channel suggests a physical basis for coupling activation to the inactivation process. Our data show that a gating perturbation of S4-DI exerts the largest effect on S4-DIV fluorescence behavior and, likewise, perturbation of S4-DIV induces a maximal shift on S4-DI movement. The reciprocity and magnitude of these long-range perturbations indicate cooperativity between the two domains. Although our data reveals S4-DIV is also coupled to the S4s of DII and DIII, the coupling strength between S4-DI and S4-DIV, as determined by the magnitude of the $DV_{1/2}$, is most significant. Previous work from different labs have shown that S4-DIV of the sodium channel plays a major role in the inactivation process and may serve to initiate the fast inactivation (Chen et al., 1996; Kontis and Goldin, 1997; Sheets et al., 1999; Chanda and Bezanilla, 2002). Together, these results suggest that the coupling between activation and inactivation may be achieved by coupling S4-DIV with the movement of other voltage sensors, notably S4-DI.

Another functional advantage conferred by cooperativity revolves around the issue of electrical signaling. During an action potential, voltage-gated sodium channels generate the rising phase that requires faster activation kinetics than K^+ channels. Consequently, multidomain eukaryotic sodium channels are typically several fold faster than potassium channels. Positive cooperativity between voltage-sensing subunits will accelerate activation kinetics as shown by a solution of the four state model depicted in Scheme I (see APPENDIX for proof). Thus, tight coupling of S4 movement in voltage-dependent sodium channels may be the basis for the rapid kinetics required for fast electrical communication.

APPENDIX

Here we provide an analytic description illustrating the effect of cooperativity on the kinetics of sodium channel activation. A four-state model of a channel consisting of two subunits is shown in Scheme I. The forward rates are denoted by α and backward rates by β, thus the equilibrium constants $K_1 = \alpha_1/\beta_1$ and $K_2 = \beta_2/\beta$. The coupling factor n is assigned a value of 1 when the movement of each subunit is completely independent of the other (i.e., uncoupled case). For simplicity, assume that a large depolarization is applied such that the forward rate constants α_1 and α_2 are much larger than the backward rate constants β_1 and β_2. Solving the rate equations, the gating current I_g is given by

$$I_g = \left\{(\alpha_1+\alpha_2) - n\alpha_1\alpha_2\frac{(\alpha_1+\alpha_2)(2-n)}{[\alpha_1+\alpha_2(1-n)][\alpha_2+\alpha_1(1-n)]}\right\} \quad (8)$$

$$\exp[-(\alpha_1+\alpha_2)t] + \frac{n\alpha_1\alpha_2}{\alpha_1+\alpha_2-n\alpha_2}$$

$$\exp[-n\alpha_2 t] + \frac{n\alpha_1\alpha_2}{\alpha_1+\alpha_2-n\alpha_1}\exp[-n\alpha_1 t].$$

Assuming $\alpha_1 = \alpha_2 = \alpha$, then we get

$$I_g = 4\alpha\frac{n-1}{n-2}\exp[-2\alpha t] - 2\alpha\frac{n}{n-2}\exp[-n\alpha t]. \quad (9)$$

The gating currents would exhibit a fast rising phase with a rate constant $n\alpha$ and a decaying phase with a rate constant 2α, twice as fast as the elementary rate constant in the absence of positive cooperativity.

When both subunits move independently ($n = 1$), the gating current in Eq. 9 is reduced to

$$I_g = 2\alpha\exp[-\alpha t]. \quad (10)$$

This is a simple exponential decay with a rate constant α and no rising phase. In the sodium channel, the opening of the channel is not rate limiting, therefore,

when gating current kinetics are accelerated, the sodium channel activation will also increase.

We thank Drs. Diane Papazian and Rikard Blunck for critically reading the previous versions of the manuscript; Benoit Roux for sharing the coordinates of the K^+ channel model. We are grateful to Rob Herman and Hongyan Guo for their technical assistance.

B. Chanda was supported by AHA postdoctoral fellowship (0225006Y), and O.K. Asamoah by NRSA predoctoral fellowship (1 F31 GM20596-03). This work was supported by NIH grant GM30376.

Olaf S. Andersen served as editor.

Submitted: 3 November 2003
Accepted: 20 January 2004

REFERENCES

Aggarwal, S.K., and R. MacKinnon. 1996. Contribution of the S4 segment to gating charge in the Shaker K^+ channel. *Neuron.* 16: 1169–1177.

Aldrich, R.W., D.P. Corey, and C.F. Stevens. 1983. A reinterpretation of mammalian sodium channel gating based on single channel recording. *Nature.* 306:436–441.

Aldrich, R.W., and C.F. Stevens. 1983. Inactivation of open and closed sodium channels determined separately. *Cold Spring Harb. Symp. Quant. Biol.* 48:147–153.

Armstrong, C.M., and F. Bezanilla. 1977. Inactivation of the sodium channel. II. Gating current experiments. *J. Gen. Physiol.* 70:567–590.

Catterall, W.A. 2000. From ionic currents to molecular mechanisms: the structure and function of voltage-gated sodium channels. *Neuron.* 26:13–25.

Cha, A., and F. Bezanilla. 1997. Characterizing voltage-dependent conformational changes in the Shaker K^+ channel with fluorescence. *Neuron.* 19:1127–1140.

Cha, A., and F. Bezanilla. 1998. Structural implications of fluorescence quenching in the Shaker K^+ channel. *J. Gen. Physiol.* 112: 391–408.

Cha, A., P.C. Ruben, A.L. George, Jr., E. Fujimoto, and F. Bezanilla. 1999. Voltage sensors in domains III and IV, but not I and II, are immobilized by Na^+ channel fast inactivation. *Neuron.* 22:73–87.

Chanda, B., and F. Bezanilla. 2002. Tracking voltage-dependent conformational changes in skeletal muscle sodium channel during activation. *J. Gen. Physiol.* 120:629–645.

Chen, L.Q., V. Santarelli, R. Horn, and R.G. Kallen. 1996. A unique role for the S4 segment of domain 4 in the inactivation of sodium channels. *J. Gen. Physiol.* 108:549–556.

Di Cera, E. 1998. Site-specific thermodynamics: Understanding cooperativity in molecular recognition. *Chem. Rev.* 98:1563–1591.

Gandhi, C.S., E. Loots, and E.Y. Isacoff. 2000. Reconstructing voltage sensor-pore interaction from a fluorescence scan of a voltage-gated K^+ channel. *Neuron.* 27:585–595.

Goldman, L., and C.L. Schauf. 1972. Inactivation of the sodium current in Myxicola giant axons. Evidence for coupling to the activation process. *J. Gen. Physiol.* 59:659–675.

Hanck, D.A., and M.F. Sheets. 1995. Modification of inactivation in cardiac sodium channels: ionic current studies with Anthopleurin-A toxin. *J. Gen. Physiol.* 106:601–616.

Hodgkin, A.L., and A.F. Huxley. 1952. A quantitative description of membrane current and its application to conduction and excitation in nerve. *J. Physiol.* 117:500–544.

Horn, R., S. Ding, and H.J. Gruber. 2000. Immobilizing the moving parts of voltage-gated ion channels. *J. Gen. Physiol.* 116:461–476.

Horrigan, F.T., and R.W. Aldrich. 1999. Allosteric voltage gating of potassium channels II. Mslo channel gating charge movement in the absence of Ca^{2+}. *J. Gen. Physiol.* 114:305–336.

Horrigan, F.T., J. Cui, and R.W. Aldrich. 1999. Allosteric voltage gating of potassium channels I. Mslo ionic currents in the absence of Ca^{2+}. *J. Gen. Physiol.* 114:277–304.

Jiang, Y., A. Lee, J. Chen, V. Ruta, M. Cadene, B.T. Chait, and R. MacKinnon. 2003. X-ray structure of a voltage-dependent K^+ channel. *Nature.* 423:33–41.

Keynes, R.D., and F. Elinder. 1998. On the slowly rising phase of the sodium gating current in the squid giant axon. *Proc. R. Soc. Lond. B. Biol. Sci.* 265:255–262.

Keynes, R.D., and J.E. Kimura. 1983. Kinetics of activation of the sodium conductance in the squid giant-axon. *J. Physiol.* 336:621–634.

Kontis, K.J., and A.L. Goldin. 1997. Sodium channel inactivation is altered by substitution of voltage sensor positive charges. *J. Gen. Physiol.* 110:403–413.

Kontis, K.J., A. Rounaghi, and A.L. Goldin. 1997. Sodium channel activation gating is affected by substitutions of voltage sensor positive charges in all four domains. *J. Gen. Physiol.* 110:391–401.

Laine, M., M.C. Lin, J.P. Bannister, W.R. Silverman, A.F. Mock, B. Roux, and D.M. Papazian. 2003. Atomic proximity between S4 segment and pore domain in Shaker potassium channels. *Neuron.* 39:467–481.

Ledwell, J.L., and R.W. Aldrich. 1999. Mutations in the S4 region isolate the final voltage-dependent cooperative step in potassium channel activation. *J. Gen. Physiol.* 113:389–414.

Li, R.A., I.L. Ennis, R.J. French, S.C. Dudley, Jr., G.F. Tomaselli, and E. Marban. 2001. Clockwise domain arrangement of the sodium channel revealed by (mu)-conotoxin (GIIIA) docking orientation. *J. Biol. Chem.* 276:11072–11077.

Liman, E.R., P. Hess, F. Weaver, and G. Koren. 1991. Voltage-sensing residues in the S4 region of a mammalian K^+ channel. *Nature.* 353:752–756.

Loots, E., and E.Y. Isacoff. 2000. Molecular coupling of S4 to a K^+ channel's slow inactivation gate. *J. Gen. Physiol.* 116:623–636.

Mannuzzu, L.M., and E.Y. Isacoff. 2000. Independence and cooperativity in rearrangements of a potassium channel voltage sensor revealed by single subunit fluorescence. *J. Gen. Physiol.* 115:257–268.

Mannuzzu, L.M., M.M. Moronne, and E.Y. Isacoff. 1996. Direct physical measure of conformational rearrangement underlying potassium channel gating. *Science.* 271:213–216.

Mitrovic, N., A.L. George, Jr., and R. Horn. 1998. Independent versus coupled inactivation in sodium channels. Role of the domain 2 S4 segment. *J. Gen. Physiol.* 111:451–462.

Mitrovic, N., A.L. George, Jr., and R. Horn. 2000. Role of domain 4 in sodium channel slow inactivation. *J. Gen. Physiol.* 115:707–718.

Noceti, F., P. Baldelli, X. Wei, N. Qin, L. Toro, L. Birnbaumer, and E. Stefani. 1996. Effective gating charges per channel in voltage-dependent K^+ and Ca^{2+} channels. *J. Gen. Physiol.* 108:143–155.

Papazian, D.M., L.C. Timpe, Y.N. Jan, and L.Y. Jan. 1991. Alteration of voltage-dependence of Shaker potassium channel by mutations in the S4 sequence. *Nature.* 349:305–310.

Patlak, J. 1991. Molecular kinetics of voltage-dependent Na^+ channels. *Physiol. Rev.* 71:1047–1080.

Patton, D.E., J.W. West, W.A. Catterall, and A.L. Goldin. 1993. A peptide segment critical for sodium channel inactivation functions as an inactivation gate in a potassium channel. *Neuron.* 11: 967–974.

Schoppa, N.E., and F.J. Sigworth. 1998. Activation of Shaker potassium channels. III. An activation gating model for wild-type and V2 mutant channels. *J. Gen. Physiol.* 111:313–342.

Seoh, S.A., D. Sigg, D.M. Papazian, and F. Bezanilla. 1996. Voltage-

sensing residues in the S2 and S4 segments of the Shaker K^+ channel. *Neuron.* 16:1159–1167.

Sheets, M.F., and D.A. Hanck. 1995. Voltage-dependent open-state inactivation of cardiac sodium channels: gating current studies with Anthopleurin-A toxin. *J. Gen. Physiol.* 106:617–640.

Sheets, M.F., J.W. Kyle, R.G. Kallen, and D.A. Hanck. 1999. The Na channel voltage sensor associated with inactivation is localized to the external charged residues of domain IV, S4. *Biophys. J.* 77: 747–757.

Smith-Maxwell, C.J., J.L. Ledwell, and R.W. Aldrich. 1998. Role of the S4 in cooperativity of voltage-dependent potassium channel activation. *J. Gen. Physiol.* 111:399–420.

Stuhmer, W., F. Conti, H. Suzuki, X.D. Wang, M. Noda, N. Yahagi, H. Kubo, and S. Numa. 1989. Structural parts involved in activation and inactivation of the sodium channel. *Nature.* 339:597–603.

Vandenberg, C.A., and F. Bezanilla. 1991. A sodium channel gating model based on single channel, macroscopic ionic, and gating currents in the squid giant axon. *Biophys. J.* 60:1511–1533.

West, J.W., D.E. Patton, T. Scheuer, Y. Wang, A.L. Goldin, and W.A. Catterall. 1992. A cluster of hydrophobic amino acid residues required for fast Na^+ channel inactivation. *Proc. Natl. Acad. Sci. USA.* 89:10910–10914.

Wyman, J., and S. Gill. 1990. Binding and Linkage: Functional Chemistry of Biological Macromolecules. 1st ed. University Science Books. Mill Valley, CA. 269–303.

Yang, N., A.L. George, Jr., and R. Horn. 1996. Molecular basis of charge movement in voltage-gated sodium channels. *Neuron.* 16: 113–122.

Yang, N., and R. Horn. 1995. Evidence for voltage-dependent S4 movement in sodium channels. *Neuron.* 15:213–218.

Zagotta, W.N., T. Hoshi, and R.W. Aldrich. 1994. Shaker potassium channel gating. III: Evaluation of kinetic models for activation. *J. Gen. Physiol.* 103:321–362.